Revisiting The Trapping of Noble Gases (He – Kr) By The Triatomic H3+ and Li3+ Species: A Density Functional Reactivity Theory Study

Xin He
Hunan Normal University
Chunna Guo
Hunan Normal University
Meng Li
Hunan Normal University
Shujing Zhong
Hunan Normal University
Xinjie Wan
Hunan Normal University
Chunying Rong
Hunan Normal University
Pratim K. Chattaraj
Indian Institute of Technology
Dongbo Zhao (dongbo@ynu.edu.cn)
Yunnan University https://orcid.org/0000-0002-0927-4361

Research Article

Keywords: Density functional theory, boron clusters, bonding, aromaticity, chemical reactivity

Posted Date: December 10th, 2021

DOI: https://doi.org/10.21203/rs.3.rs-1115957/v1

Version of Record: A version of this preprint was published at Journal of Molecular Modeling on April 19th, 2022. See the published version at https://doi.org/10.1007/s00894-022-05099-7.

Revisiting the Trapping of Noble Gases (He – Kr) by the Triatomic H_3^+ and Li_3^+ Species: A Density Functional Reactivity Theory Study

Xin He,[1] Chunna Guo,[1] Meng Li,[1] Shujing Zhong,[1] Xinjie Wan,[1] Chunying Rong,[1,*]

Pratim K. Chattaraj,[2,*] and Dongbo Zhao,[3,*]

[1]*Key Laboratory of Light Energy Conversion Materials of Hunan Province College, Hunan Normal University, Changsha, Hunan 410081, P.R. China.*

E-mail*:* rongchunying@aliyun.com

[2]*Department of Chemistry, Indian Institute of Technology, Kharagpur 721302, India.*

E-mail*:* pkc@chem.iitkgp.ac.in

[3]*Institute of Biomedical Research, Yunnan University, Kunming 650500, Yunnan, P.R. China.*

E-mail: dongbo@ynu.edu.cn

Abstract

Small atomic clusters with exotic stability, bonding, aromaticity and reactivity properties can be made use of for various purposes. In this work, we revisit the trapping of noble gas atoms (He – Kr) by the triatomic H_3^+ and Li_3^+ species by using some analytical tools from density functional theory, conceptual density functional theory, and the information-theoretic approach. Our results showcase that though similar in geometry, H_3^+ and Li_3^+ exhibit markedly different behaviour in bonding, aromaticity, and reactivity properties after the addition of noble gas atoms. Moreover, the exchange-correlation interaction and steric effect are key energy components in stablizing the clusters. This study also finds that the origin of the molecular stability of these species is due to the spatial delocalization of the electron density distribution. Our work provides an additional arsenal towards better understanding of small atomic clusters capturing noble gases.

Keywords: Density functional theory; boron clusters; bonding; aromaticity; chemical reactivity

1. Introduction

During the past few decades, atomic clusters have been the subject of intensive research due to their indispensable roles in biomedicine, optics and synthetic materials.[1–3] Since Bartlett first synthesized $Xe^{+}[PtF_6]^{-}$,[4] the underexplored chemistry of noble gases has witnessed rapid developments, motivating both synthetic and theoretical chemists jumping into this field.[5] It has found that noble gas insertion compounds play an important role because of their unique properties in geometrical structure, molecular stability, bonding, chemical reactivity, and other physicochemical properties.

In continuation with our previous work,[6] we intend to revisit the trapping of noble gases by H_3^{+} and Li_3^{+} species from the perspective of stability, bonding, aromaticity, and reactivity properties using the framework of conceptual density functional theory (CDFT) augmented by the information-theoretic approach (ITA). Also employed are well-established analytical tools, such as aromaticity descriptors NICS (nucleus independent chemical shift) and GIMIC (gauge-including magnetically induced currents), “spike” region for noncovalent interactions and our newly developed analytical tools in analyzing strong covalent interactions and reactivity patterns in terms of local temperatures, that are intrinsically different from their thermodynamic definitions. Combining these effective methods allows us to gain insights into these species and to obtain many unexpected properties of these small atomic clusters.

2. Methodology

In Kohn-Shan DFT, we can decompose the total energy difference (ΔE) into its components as[7,8]

$$\Delta E[\rho] = \Delta T_s[\rho] + \Delta E_e[\rho] + \Delta E_{xc}[\rho] \qquad (1)$$

and

$$\Delta E[\rho] = \Delta E_s[\rho] + \Delta E_e[\rho] + \Delta E_q[\rho] \qquad (2)$$

where T_s, E_e, and E_{xc} are the noninteracting kinetic, electrostatic, and exchange−correlation energies, respectively. The electrostatic energy E_e includes three independent components: the nuclear−electron attraction, V_{ne}; the classical interelectron Coulombic repulsion, J; and the nuclear−nuclear repulsion, V_{nn}. The last term E_{xc} consists of exchange (E_x) and correlation (E_c) components. E_s stands for the energetic contribution from the steric effect, and E_q signifies the contribution originating from Fermionic quantum effect (due to the exchange−correlation interaction). The steric effect E_s has been shown to be simply the Weizsäcker kinetic energy as will be shown later in Eq. (8). The definition of E_q is by simply combining Eqs. (1), (2) and (8), which reads

$$\Delta E_q[\rho] = \Delta E_{xc}[\rho] + \Delta T_s[\rho] - \Delta E_s[\rho] \qquad (3)$$

This new formulation has its own distinct physical meaning with a corresponding physical state.[8] It has been applied to a number of molecular systems and phenomena, such as conformational changes,[8–13] anomeric effect,[14–16] the *cis*-effect,[17] , etc. The results are consistent with our chemical intuition and conventional wisdom.

In CDFT,[18–20] besides the well-known local descriptor Fukui function[21,22],

we very recently evaluated the local temperature $T(\mathbf{r})$[23] of a molecule using the kinetic energy density (KED),

$$T(\mathbf{r}) = \frac{2\tau(\mathbf{r})}{3k_{\mathrm{B}}} \qquad (4)$$

where $\tau(\mathbf{r})$, $\rho(\mathbf{r})$, and k_{B} are the KED, electron density, and Boltzmann constant, respectively. Among various KEDs, two well-appreciated definitions are the Hamiltonian KED

$$\tau(\mathbf{r}) = -\frac{1}{2}\sum_i \phi_i^*(\mathbf{r})\,\nabla^2\phi_i(\mathbf{r}) \qquad (5)$$

with $\varphi_i(\mathbf{r})$ as the occupied Kohn−Sham orbitals, and the Lagrangian KED

$$\tau(\mathbf{r}) = \frac{1}{2}\sum_i \phi_i^*(\mathbf{r})\,\nabla\phi_i(\mathbf{r}) = -\frac{1}{2}\sum_i \phi_i^*(\mathbf{r})\,\nabla^2\phi_i(\mathbf{r}) + \frac{1}{4}\nabla^2\rho(\mathbf{r}) \qquad (6)$$

where $\nabla^2\rho(\mathbf{r})$ is the Laplacian of the electron density. In addition, in the literature [24–29] there exist two famous approximate forms of KEDs: the Thomas−Fermi formula (derived for the homogeneous electron gas) and the Weizsäcker KED (exact for one-electron and two-electron Hartree-Fock systems), as defined by Eqs. (7) and (8), respectively:

$$\tau_{\mathrm{TF}}(\mathbf{r}) = 3/5\,(6\pi^2)^{2/3}\rho(\mathbf{r})^{5/3} \qquad (7)$$

$$\tau_{\mathrm{W}}(\mathbf{r}) = \frac{1}{8}\frac{|\nabla\rho(\mathbf{r})|^2}{\rho(\mathbf{r})} \qquad (8)$$

Very recently, based on the early work of Ghosh and Parr[30,31] and inspired by the definition of Fukui function, we proposed to employ the local temperature to appreciate chemical reactivity. For nucleophilic attack, using the local temperature, we define

$$\theta^+(\mathbf{r}) = \left(\frac{\partial T(\mathbf{r})}{\partial N}\right)^+_{v(\mathbf{r})} = T_N(\mathbf{r}) - T_{N+1}(\mathbf{r}) \qquad (9)$$

and for electrophilic attack, we define

$$\theta^{-}(\mathbf{r}) = \left(\frac{\partial T(\mathbf{r})}{\partial N}\right)^{-}_{v(\mathbf{r})} = T_{N-1}(\mathbf{r}) - T_N(\mathbf{r}) \qquad (10)$$

where T_N, T_{N+1}, and T_{N-1} are local temperatures for the system with N, $N + 1$, and $N - 1$ electrons, respectively, in the N electron (fixed) geometry. Condensed-to-atom local temperatures were also defined. An in-depth discussion and applications of local temperatures can be found in our recent publication.[23] The uniqueness of the descriptor of local temperature is manifold, compared to its predecessor Fukui function. The scope of applications is greatly expanded due to its connection to the information theory. Moreover, the local temperature can be used to explore bonding (through a relevant quantum topology analysis), especially for weakly bonded systems as it is based on the KDE. Similar examples are the well-known electron localization function (ELF)[32,33], as devised to identify the localization of electron pairs, and our recently proposed SCI (strong covalent interaction) index,[34] which can be used to determine multiple bond orders (up to quintuple bond). Suffice to note that CDFT is still an active field with lots of progresses keep emerging.

Next, we will give a brief introduction to ELF and SCI. Earlier, we assumed that the areas forming multiple covalent bonds should experience strong repulsions due to the existence of the Pauli exclusion principle, and proposed the SCI index to identify multiple covalent bonds.[34] The Pauli energy (E_P)[35] is defined as

$$E_{\mathrm{P}}[\rho(\mathbf{r})] \equiv \int t_{\mathrm{P}}(\mathbf{r})d\mathbf{r} = T_{\mathrm{S}}[\rho(\mathbf{r})] - T_{\mathrm{W}}[\rho(\mathbf{r})] \equiv \int (t_{\mathrm{S}}(\mathbf{r}) - t_{\mathrm{W}}(\mathbf{r}))d\mathbf{r} \qquad (11)$$

$$T_{\mathrm{W}}[\rho(\mathbf{r})] \equiv \int t_{\mathrm{W}}(\mathbf{r})\, d\mathbf{r} = \frac{1}{8}\int \frac{|\nabla\rho(\mathbf{r})|^2}{\rho(\mathbf{r})} d\mathbf{r} \qquad (12)$$

with the Weizsäcker kinetic energy T_W as defined in Eq. (12), T_S as the total noninteracting kinetic energy, and $t_S(\mathbf{r})$ and $t_P(\mathbf{r})$ the corresponding local energy

density. To convert the Pauli energy to a dimensionless quantity, we define a local function $\zeta(\mathbf{r})$,[34]

$$\zeta(\mathbf{r}) \equiv \frac{t_{\mathrm{P}}(\mathbf{r})}{t_{\mathrm{TF}}(\mathbf{r})} = \frac{t_{\mathrm{S}}(\mathbf{r}) - t_{\mathrm{W}}(\mathbf{r})}{t_{\mathrm{TF}}(\mathbf{r})} \qquad (13)$$

and then the SCI index is defined as the reciprocal of $\zeta(\mathbf{r})$,[34]

$$\mathrm{SCI} = \frac{1}{\zeta(\mathbf{r})} \qquad (14)$$

This index is similar to the ELF (electron localization function) index,[32,33]

$$\mathrm{ELF} = \frac{1}{1+\zeta^2(\mathbf{r})} \qquad (15)$$

We have to mention that the SCI index has its own unique features compared to that of ELF. While ELF was defined to identify localized regions, the SCI index has a clear physical meaning of the Pauli energy contribution. We have also revealed that our SCI results are consistent. For example, a double covalent bond always exhibits a dumbbell signature isosurface, and a donut or torus for a triple covalent bond.[34] For systems with complex bond types, one can predict their covalent bond multiplicity based on the signature isosurfaces. More examples about SCI index applications can be found elsewhere.[36]

3. Computational Details

Starting from the equilateral triangle H_3^+ and Li_3^+,[37,38] we gradually added one, two, and three noble gas atoms, leading to a total of 26 systems in this work. All quantum chemical calculations (structure optimization, vibrational analysis, etc.) were performed with the Gaussian 16 package[39] at the B3LYP/aug-cc-pVTZ level[40–42] of theory with default ultrafine integration grids and tight self-consistent field convergence criteria to rule out numerical noises. Molecular

wavefunctions were fed into the Multiwfn 3.8 program[43] to evaluate the SCI index, ITA quantities, local temperatures, and noncovalent interactions (NCI). To assess aromaticity characteristics of a planar structure, we apply NICS (nucleus independent chemical shift)[44] and GIMIC (gauge-including magnetically induced currents)[45] for this purpose. Our previous studies[46–52] have demonstrated their effectiveness and reliability for other systems. Details of their definitions and applications can be found elsewhere.[53,54] The total energy components were obtained with the keyword of iop(5/33=1).

4. Results and Discussion

We first take a look at the noncovalent interactions (NCI)[55] and strong covalent interactions (SCI)[34] of all systems with $[H_3Kr_3]^+$ and $[Li_3Kr_3]^+$ as an illustration (Figure 1). In Figures 1a and 1d, one can clearly observe a "spike" region somewhere in the vicinity of zero both for $[H_3Kr_3]^+$ and $[Li_3Kr_3]^+$, indicative of very weak, attractive van der Waals interactions. But where do they come from? One can see that for $H_3Kr_3^+$ (in Figure 1b), the NCI isosurface mainly lies between the H and Kr atoms; for $[Li_3Kr_3]^+$ (in Figure 1e), both interatomic Li-Kr and Li-Li interactions are noncovalent in nature. The observation is in line with our previous work of "bare" H_3^+ and Li_3^+. Furthermore, in Figures 1c and 1f, no signature of SCI isosurface for double or triple or other bonds is observed, indicating that there is no obvious strong covalent bond.

Next, we will delve into the aromaticity of the H_3^+ and Li_3^+ clusters and the corresponding trapped noble gas clusters. It is well-documented in the literature that a negative NICS value indicates the existence of aromaticity. We clearly know that H_3^+

and Li_3^+ structures are aromatic, though Li_3^+ is not σ-aromatic in nature.[56,57]. Does the addition of noble gases change its aromaticity? Collected in Table 1 are the NICS(0), NICS(1) and $NICS(1)_{zz}$ values, which are all negative, indicating that the each trapped cluster is still aromatic after noble gas atoms are added. One can also see that as the atomic radii of noble gases increase, the NICS values simultaneously decrease. For example, the values of NICS(0) are –33.75, –32.86, –31.74, –22.37 ppm for H_3^+, $He_3H_3^+$, $Ne_3H_3^+$, $Ar_3H_3^+$, and $Kr_3H_3^+$, respectively. The similar trend is observed for Li_3^+ and its trapped noble gas clusters. In addition, we employ the GIMIC diagrams as shown in Figure 2 to determine aromaticity/anti-aromaticity. It is lucidly shown that all currents run in a counterclockwise manner, which is indicative of aromaticity. It is worthwhile to note that for H_3^+ and its trapped noble gas clusters, sparsity of current distributions around the H_3^+ local motif is in line with the decreased NICS values as previously mentioned. However, this is not the case with Li_3^+. One possible reason is that H_3^+ is assembled together because of electron delocalization but for Li_3^+ it is weak van der Waals interactions that counts.[56] In a nutshell, addition of noble gas atoms to H_3^+ and Li_3^+ leads to different aromaticity properties.

We employ the local CDFT descriptors, the Fukui function and the local temperature, to unveil the possible electrophilic and nucleophilic sites of a molecular system. Shown in Figure 3 are the Fukui function and local temperature results for HeH_3^+ and $HeLi_3^+$. One can see that the overall trend for the Fukui function and the local temperature is similar. For $HeHe_3^+$ (see Figure 3A), the electrophilic (Θ^-/f^-) and nucleophilic (Θ^+/f^+) sites are located at the He nucleus and the H_3 motif, respectively.

However, the trend is reversed for electrophilic (Θ^-/f^-) attacks of $HeLi_3^+$. Moreover, the electrophilic local temperature is more localized than the Fukui function for HeH_3^+ as shown in Figure 3B (upper panel). This indicates that the local temperature is a more definitive quantity in determining the reactivity sites of a molecular system. To summarize, though similar in geometry structures, HeH_3^+ and $HeLi_3^+$ can have very different chemical reactivity behavior.

We further dissect the molecular stability of all the noble gas trapping clusters by H_3^+ and Li_3^+. A total of 12 possible chemical reactions for each of them are proposed as shown in Table 2 by gradually adding a noble gas atom. Collected in Table 2 are the total energy difference (ΔE) and its components as well as the enthalpy difference (ΔH). One can see that ΔH is very close to ΔE and thereafter we only concentrate on ΔE. From Table 2, several points can be made accordingly. (i) The total energy difference is negative for all systems indicating that addition of noble gas atoms to the H_3^+ and Li_3^+ motifs is energetically favorable. (ii) Adding the noble gas atoms to H_3^+ is relatively easier than to Li_3^+ as evidenced by the total energy difference. (iii) In addition, we find that it becomes much more difficult to add more than one noble gas atoms to H_3^+, especially for Ar and Kr. For example, when one adds only one Kr atom to the H_3^+ motif, the ΔE is –73.1 kJ/mol. If one more Kr atom is added, the ΔE value becomes –19.8 kJ/mol. However, this is not the case for Li_3^+ and the corresponding two energy differences are –15.2 and –13.8 kJ/mol respectively. One possible reason for the discrepancy lies in the bonding patterns in H_3^+ and Li_3^+.[56] A more stable substrate leads to a more stable complex.

From Table 2, we find that the exchange-correlation (ΔE_{xc}) part is negative, indicative of its positive role in stabilizing the complex. The negative steric hindrance (ΔE_s) is largely compensated by the positive quantum effect (ΔE_q). What is the origin and nature of molecular stability? In other words, is there a single energetic component that is mostly responsible for the molecular stability of these systems? Shown in Figure 4 are the strong correlations between the total energy difference and the exchange-correlation (ΔE_{xc}) and the steric hindrance (ΔE_s), as well as ITA quantities, Shannon entropy (ΔS_S)[58] and Fisher information (ΔI_F)[59], whose values are given in Table 3. In a nutshell, from the viewpoint of energetics, it is the exchange-correlation that is essentially responsible for the total energy difference, which is a good supplement to our previous publications where the electrostatic potential (ΔE_e) dominated. Moreover, from the perspective of information theory, spatial delocalization of the electron density gauged by the Shannon entropy is the origin of the molecular stability of these trapping clusters. This result provides us a novel insight into this complicated phenomenon of molecular stability associated with intermolecular interactions. Similar results have been reported by us for isomeric (intramolecular) stability of fullerene buckyballs.[60]

Finally, we also tabulate some ITA quantities (GBP entropy S_{GBP}[30] and information gain ΔI_G[61,62]) in Table 3 and the correlation coefficient (R) between the total energy and its components with ITA quantities as shown in Table 4. It is known that ITA and energetic quantities can be strongly intercorrelated.[63–65] These different but strongly correlated relationships provide effective measurements

about the electron density distribution of the systems; thus, they attribute useful and novel insights into the nature and origin of various physicochemical phenomena, including isomeric stability of fullerenes and trapping noble gas clusters as in this work.

5. Conclusions

To summarize, in this work, we present the results of bonding, aromaticity and reactivity properties for the trapping of noble gas atoms (He–Kr) by the triatomic H_3^+ and Li_3^+ species from certain theoretical and analytical tools. Though similar in geometrical structure, the trapping noble gas clusters of H_3^+ and Li_3^+ differ much in bonding, aromaticity, and reactivity properties. The core reason lies in the structural motifs of H_3^+ and Li_3^+. We further analyzed the origin and nature of the molecular stability in terms of energetics and information theory. We have shown that it is the exchange-correlation interaction and steric effect that are responsible for the total molecular stability. Shannon entropy results corroborate that electron delocalization is the origin of the molecular stability. We mention in passing that more future studies along this direction will help us better appreciate atomic clusters with many unconventional properties and unveil many novel and potential applications.

Declarations

Funding: SJZ and CYR acknowledge support from the science and technology

innovation Program of Hunan Province (2021RC1003). PKC would like to thank DST, New Delhi, India for the J. C. Bose National Fellowship, grant number SR/S2/JCB-09/2009. DBZ was supported by the startup funding of Yunnan university.

Competing interests: The authors declare no competing interests.

Availability of data and material: All data in this work are in the text.

Code availability: No new code is generated from this work.

Authors' contributions: P.K.C., C.Y.R., and D.B.Z. conceived and designed the overall project. X.H., C.N.G., M.L., S.J.Z., and X.J.W. carried out the computational studies. X.H., P.K.C., and D.B.Z. analyzed the data and wrote the manuscript with the input of all authors. All authors edited and approved the manuscript.

References

1. Fan Y, Liu S, Yi Y, Rong H, Zhang J (2021) Catalytic Nanomaterials toward Atomic Levels for Biomedical Applications: From Metal Clusters to Single-Atom Catalysts. ACS Nano 15:2005–2037

2. Philip R, Chantharasupawong P, Qian H, Jin RC, Thomas J (2012) Evolution of Nonlinear Optical Properties: From Gold Atomic Clusters to Plasmonic Nanocrystals. Nano Lett 12:4661–4667

3. Jena P, Sun Q (2018) Super Atomic Clusters: Design Rules and Potential for Building Blocks of Materials. Chem Rev 118:5755–5870

4. Bartlett N (1962) Xenon hexafluoroplatinate(V) $Xe^{+}[PtF_6]^{-}$. Proc Chem Soc 115:218

5. Miller S, Tennyson J, Geballe TR, Stallard T (2020) Thirty years of H_3^+ astronomy. Rev Mod Phys 92:035003

6. Chakraborty A, Giri S, Chattaraj PK (2010) Trapping of noble gases (He–Kr) by the aromatic H_3^+ and Li_3^+ species: a conceptual DFT approach. New J Chem 34:1936–1945

7. Parr RG, Yang WT (1989) Density functional theory for atoms and molecules. Oxford University Press, New York

8. Liu SB (2007) Steric effect: A quantitative description from density functional theory. J Chem Phys 126:244103

9. Liu SB, Govind N (2008) Toward understanding the nature of internal rotation barriers with a new energy partition scheme: ethane and n-butane. J Phys Chem A 112:6690–6699

10. Liu SB, Govind N, Pedersen LG (2008) Exploring the origin of the internal rotational barrier for molecules with one rotatable dihedral angle. J Chem Phys 129:094104

11. Liu SB, Hu H, Pedersen LG (2010) Steric, quantum, and electrostatic effects on S_N2 reaction barriers in gas phase. J Phys Chem A 114:5913–5918

12. Ess DH, Liu SB, De Proft F (2010) Density functional steric analysis of linear and branched alkanes. J Phys Chem A 114:12952–12957

13. Liu SB (2013) Origin and nature of bond rotation barriers: a unified view. J Phys Chem A 117:962–965

14. Huang Y, Zhong AG, Yang QS, Liu SB (2011) Origin of anomeric effect: a density functional steric analysis. J Chem Phys 134:084103

15. Zhou XY, Yu DH, Rong CY, Lu T, Liu SB (2017) Anomeric effect revisited: perspective from information-theoretic approach in density functional reactivity theory. Chem Phys Lett 694:97–102

16. Cao XF, Liu SQ, Rong CY, Lu T, Liu SB (2017) Is there a generalized anomeric effect? Analyses from energy components and information-theoretic quantities from density functional reactivity theory. Chem Phys Lett 687:131–137

17. Zhao DB, Rong CY, Jenkins S, Kirk SR, Yin DL, Liu SB (2013) Origin of the *cis*-effect: a density functional theory study of doubly substituted ethylenes. Acta Phys-Chim Sin 29:43–54

18. Geerlings P, De Proft F, Langenaeker W (2003) Conceptual Density Functional Theory. Chem Rev 103:1793–1874

19. Chattaraj PK, Sarkar U, Roy DR (2006) Electrophilicity Index. Chem Rev 106:2065–2091

20. Liu SB (2009) Conceptual Density Functional Theory and Some Recent Developments.

Acta Phys-Chim Sin 25:590–600

21. Parr RG, Yang WT (1984) Density functional approach to the frontier-electron theory of chemical reactivity. J Am Chem Soc 106:4049–4050

22. Ayers PW, Levy M (2000) Perspective on “Density functional approach to the frontier-electron theory of chemical reactivity”. Theor Chem Acc 103:353–360

23. Guo CN, He X, Rong CY, Lu T, Liu SB, Chattaraj PK (2021) Local Temperature as a Chemical Reactivity Descriptor. J Phys Chem Lett 12:5623–5630

24. Garcia-Aldea D, Alvarellos JE (2007) Kinetic energy density study of some representative semilocal kinetic energy functionals. J Chem Phys 127:144109

25. Thakkar (1992) Comparison of kinetic-energy density functionals. Phys Rev A: At Mol Opt Phys 46:6920–6924

26. Salazar EX, Guarderas PF, Ludena EV, Cornejo MH, Karasiev VV (2016) Study of some simple approximations to the non-interacting kinetic energy functional. Int J Quantum Chem 116:1313–1321

27. Laricchia S, Fabiano E, Constantin LA, Della Sala F (2011) Generalized Gradient Approximations of the Noninteracting Kinetic Energy from the Semiclassical Atom Theory: Rationalization of the Accuracy of the Frozen Density Embedding Theory for Nonbonded Interactions. J Chem Theory Comput 7:2439–2451

28. Constantin LA, Fabiano E, Della Sala F (2017) Modified Fourth-Order Kinetic Energy Gradient Expansion with Hartree Potential-Dependent Coefficients. J Chem Theory Comput 13:4228–4239

29. Nafziger J, Jiang K, Wasserman A (2017) Accurate Reference Data for the Nonadditive, Noninteracting Kinetic Energy in Covalent Bonds. J Chem Theory Comput 13:577–586

30. Ghosh SK, Berkowitz M, Parr RG (1984) Transcription of ground-state density-functional theory into a local thermodynamics. Proc Natl Acad Sci U S A 81:8028–8031

31. Ghosh SK, Parr RG (1986) Phase-space approach to the exchange-energy functional of density-functional theory. Phys Rev A 34:785–791

32. Becke AD, Edgecombe K (1990) A simple measure of electron localization in atomic and molecular systems. J Chem Phys 92:5397–5403

33. Silvi B, Savin A (1994) Classification of chemical bonds based on topological analysis of electron localization functions. Nature 371:683–686

34. Liu SB, Rong CY, Lu T, Hu H (2018) Identifying Strong Covalent Interactions with Pauli Energy. J Phys Chem A 122:3087–3095

35. Holas A, March NH (1991) Construction of the Pauli potential, Pauli energy, and effective potential from the electron density. Phys Rev A: At Mol Opt Phys 44:5521–5536

36. Huang Y, Liu LH, Rong CY, Lu T, Ayers PW, Liu SB (2018) SCI: a robust and reliable density-based descriptor to determine multiple covalent bond orders. J Mol Model 24:213

37. Gaillard MJ, Gemmell DS, Goldring G, Levine I, Pietsch WJ, Poizat JC, Ratkowski AJ, Remillieux J, Vager Z, Zabransky BJ (1978) Experimental determination of the structure of H_3^+. Phys Rev A 17:1797–1803

38. Alexandrova AN, Boldyrev AI (2003) σ-Aromaticity and σ-Antiaromaticity in Alkali Metal and Alkaline Earth Metal Small Clusters. J Phys Chem A 107:554–560

39. Frisch MJ, Trucks GW, Schlegel HB, et al (2016) Gaussian 16, revision A.03. Gaussian Inc, Wallingford

40. Becke AD (1993) Density-functional thermochemistry. III the role of exact exchange. J Chem Phys 98:5648–5652

41. Lee C, Yang WT, Parr RG (1988) Development of the Colle-Salvetti correlation-energy formula into a functional of the electron density. Phys Rev B 37:785–789

42. Dunning TH Jr. (1989) Gaussian basis sets for use in correlated molecular calculations. I. The atoms boron through neon and hydrogen. J Chem Phys 90:1007–1023

43. Lu T, Chen FW (2012) Multiwfn: A multifunctional wavefunction analyzer. J Comput Chem 33:580–592

44. Schleyer PvR, Maerker C, Dransfeld A, Jiao H, van Eikema Hommes NJR (1996) Nucleus-Independent Chemical Shifts: A Simple and Efficient Aromaticity Probe. J Am Chem Soc 118:6317–6318

45. Juselius J, Sundholm D, Gauss J (2004) Calculation of current densities using gauge-including atomic orbitals. J Chem Phys 121:3952–3963

46. He X, Yu DH, Wu JY, Wang B, Rong CY, Chattaraj PK, Liu SB (2020) Towards understanding metal aromaticity in different spin states: A density functional theory and information-theoretic approach analysis. Chem Phys Lett 761:138065

47. Yu DH, Rong CY, Lu T, Chattaraj PK, De Proft F, Liu SB (2017) Aromaticity and antiaromaticity of

substituted fulvene derivatives: perspectives from the information-theoretic approach in density functional reactivity theory. Phys Chem Chem Phys 19:18635–18645

48. Yu DH, Rong CY, Lu T, De Proft F, Liu SB (2018) Baird's Rule in Substituted Fulvene Derivatives: An Information-Theoretic Study on Triplet-State Aromaticity and Antiaromaticity. ACS Omega 3:18370–18379

49. Yu DH, Rong CY, Lu T, De Proft F, Liu SB (2018) Aromaticity Study of Benzene-Fused Fulvene Derivatives Using the Information-Theoretic Approach in Density Functional Reactivity Theory. Acta Phys-Chim Sin 34:639–649

50. Yu DH, Rong CY, Lu T, Geerlings P, Proft FD, Alonso M, Liu SB (2020) Switching between Hückel and Möbius aromaticity: a density functional theory and information-theoretic approach study. Phys Chem Chem Phys 22:4715–4730

51. Yu DH, Stuyver T, Rong CY, Alonso M, Lu T, De Proft F, Geerlings P, Liu SB (2019) Global and local aromaticity of acenes from the information-theoretic approach in density functional reactivity theory. Phys Chem Chem Phys 21:18195–18210

52. Zhao DB, He X, Li M, Wang B, Guo CN, Rong CY, Chattaraj PK, Liu SB (2021) Density functional theory studies of boron clusters with exotic properties in bonding, aromaticity and reactivity. Phys Chem Chem Phys 23:24118–24124

53. Stanger A (2010) Obtaining Relative Induced Ring Currents Quantitatively from NICS. J Org Chem 75:2281–2288

54. Stanger A (2006) Nucleus-Independent Chemical Shifts (NICS): Distance Dependence and Revised Criteria for Aromaticity and Antiaromaticity. J Org Chem 71:883–893

55. Johnson ER, Keinan S, Mori-Sánchez P, Contreras-García J, Cohen AJ, Yang WT (2010) Revealing noncovalent interactions. J Am Chem Soc 132:6498–6506

56. Zhao DB, He X, Li M, Guo CN, Rong CY, Chattaraj PK, Liu SB (2021) A Density Functional Theory Study of H_3^+ and Li_3^+ Clusters: Similar Structures with Different Bonding, Aromaticity, and Reactivity Properties. *in press*.

57. Havenith RWA, Proft FD, Fowler PW, Geerlings P (2005) σ-Aromaticity in H_3^+ and Li_3^+: Insights from ring-current maps. Chem Phys Lett 407:391–396

58. Shannon CE (1948) A Mathematical Theory of Communication. Bell Syst Tech J 27:379–423

59. Fisher RA Theory of Statistical Estimation. (1925) Math Proc Cambridge Philos Soc 22:700–

725

60. Zhao DB, Liu SY, Rong CY, Zhong AG, Liu SB (2018) Toward Understanding the Isomeric Stability of Fullerenes with Density Functional Theory and the Information-Theoretic Approach. ACS Omega 3:17986–17990

61. Liu SB (2016) Information-theoretic approach in density functional reactivity theory. Acta Phys-Chim Sin 32:98–118

62. Liu SB (2019) Identity for Kullback-Leibler Divergence in Density Functional Reactivity Theory. J Chem Phys 151:141103

63. He X, Li M, Yu DH, Wang B, Zhao DB, Rong CY, Liu SB (2021) Conformational changes for porphyrinoid derivatives: an information-theoretic approach study. Theor Chem Acc 140:123

64. Li M, He X, Chen J, Wang B, Liu SB, Rong CY (2021) Density Functional Theory and Information-Theoretic Approach Study on the Origin of Homochirality in Helical Structures. J Phys Chem A 125:1269–1278

65. Liu SB (2021) Principle of Chirality Hierarchy in Three-Blade Propeller Systems. J Phys Chem Lett 12:8720–8725

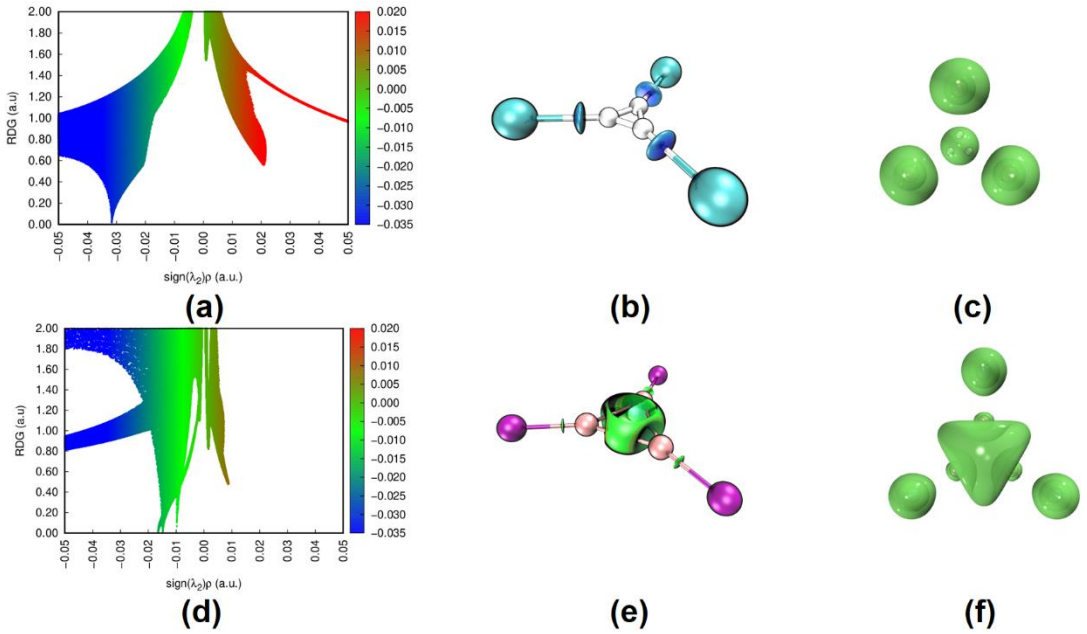

Figure 1. Noncovalent interactions (NCI) and strong covalent interactions (SCI) for upper panel $[H_3Kr_3]^+$ and lower panel $[Li_3Kr_3]^+$.

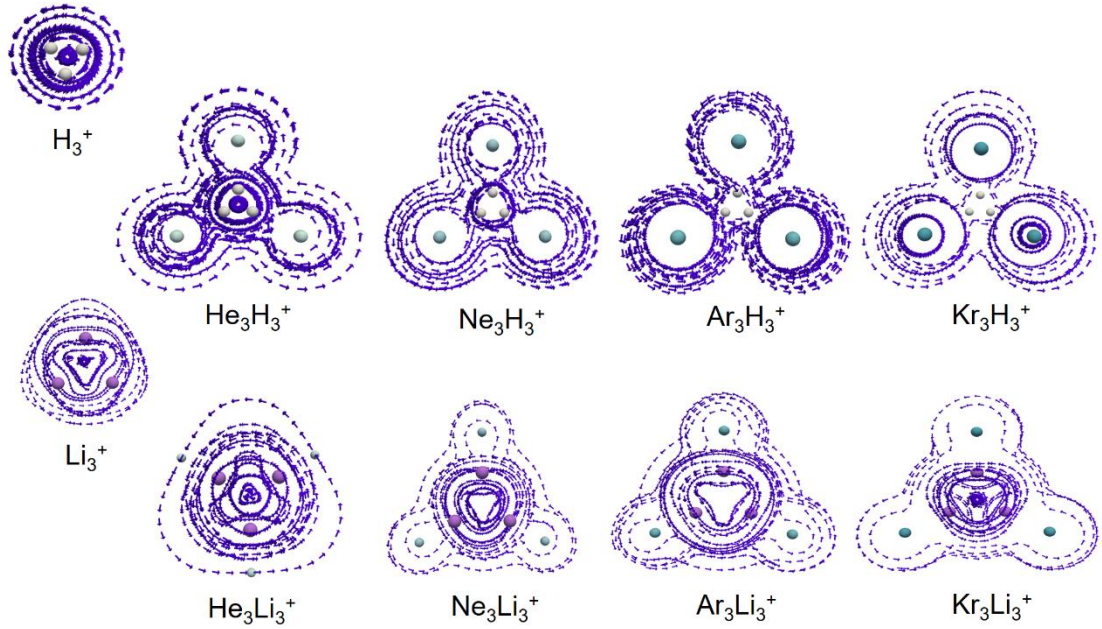

Figure 2. GIMIC distributions of upper panel H_3^+ and corresponding trapped noble gas clusters; lower panel Li_3^+ and corresponding trapped noble gas clusters from three different views.

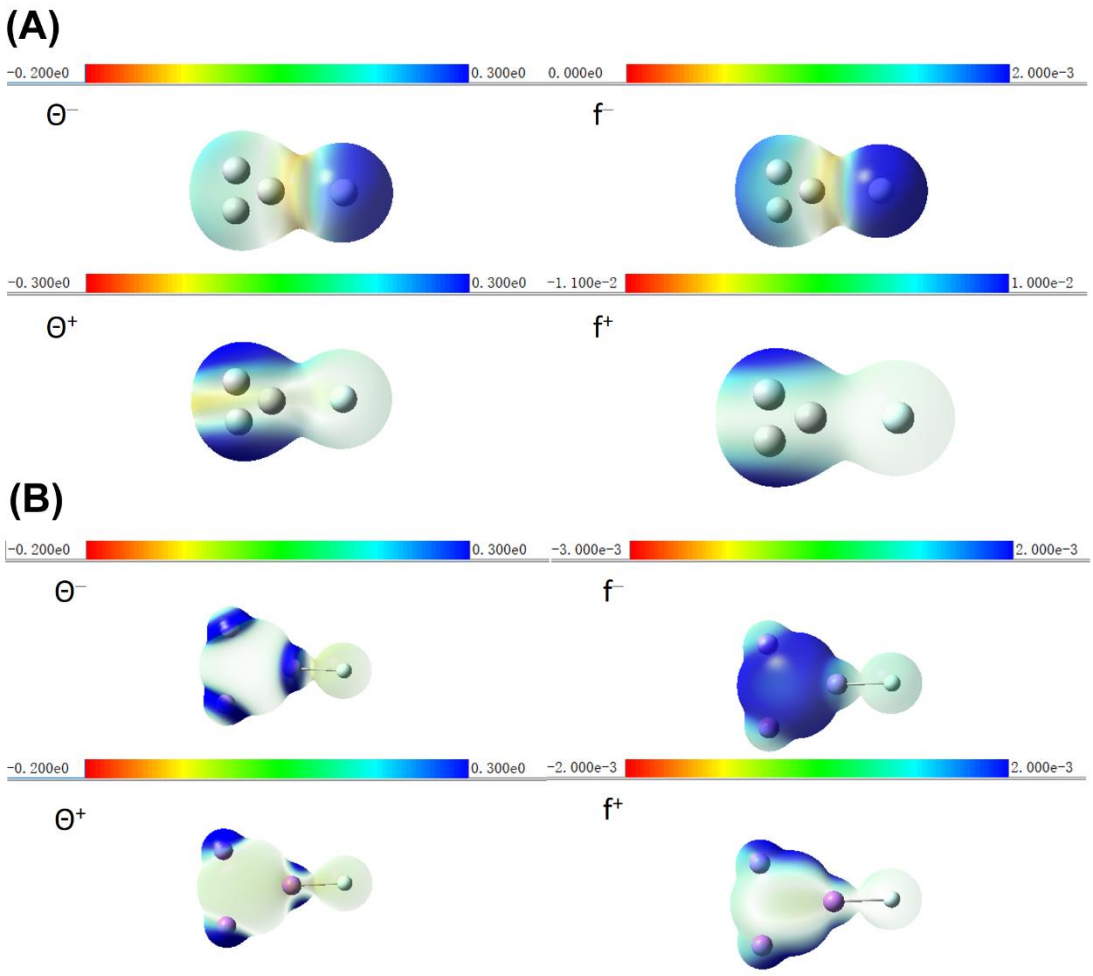

Figure 3. Electrophilic (Θ^-/f^-) and nucleophilic (Θ^+/f^+) local temperature and Fukui functions for upper panel (A) HeH_3^+ and lower panel (B) $HeLi_3^+$, mapped onto the surface of molecular density with an isovalue of 0.004 au.

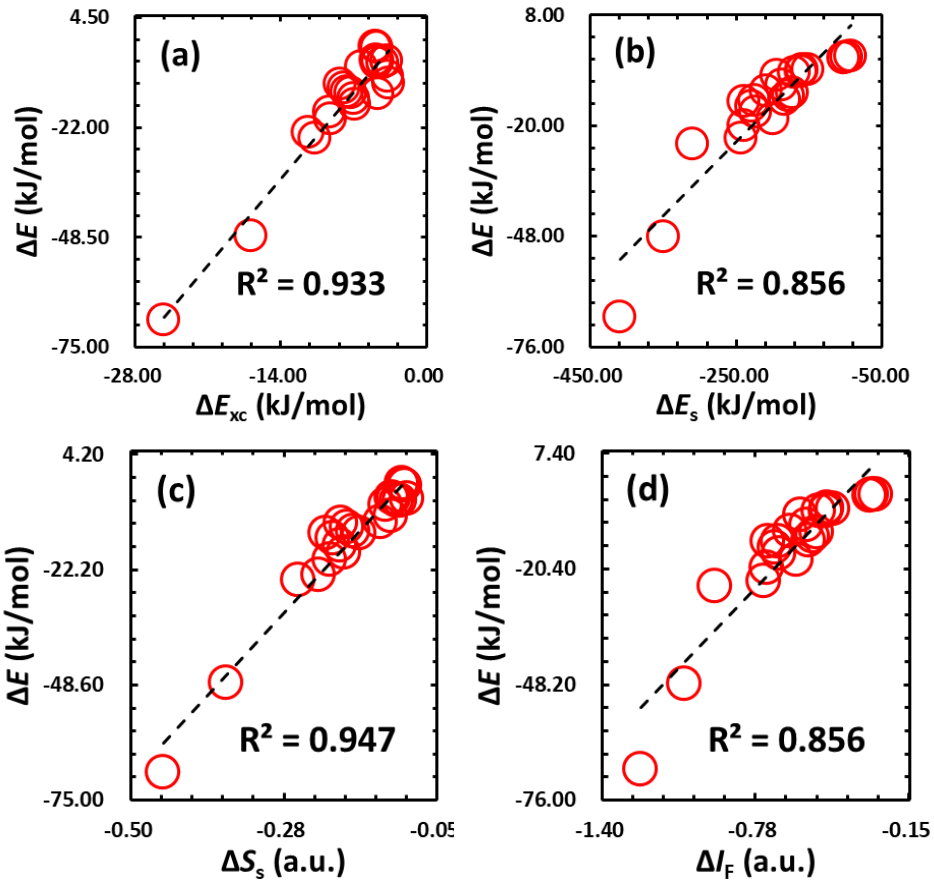

Figure 4. Strong correlations between the total energy difference (ΔE) and (a) the exchange-correlation potential (ΔE_{xc}), (b) steric hindrance (ΔE_S), (c) Shannon entropy (ΔS_S), and (d) Fisher information (ΔI_F).

Table 1. NICS(0), NICS(1) and NICS(1)$_{zz}$ values of H_3^+ and Li_3^+ and corresponding trapped noble gas clusters. Units are in ppm.

Molecule	NICS(0)	NICS(1)	NICS(1)$_{zz}$	Molecule	NICS(0)	NICS(1)	NICS(1)$_{zz}$
H_3^+	–33.75	–2.16	–7.94	Li_3^+	–11.06	–6.73	–7.26
HeH_3^+	–33.34	–2.09	–7.56	$HeLi_3^+$	–10.97	–6.69	–7.07
$He_2H_3^+$	–33.05	–2.04	–7.26	$He_2Li_3^+$	–10.89	–6.65	–6.88
$He_3H_3^+$	–32.86	–2.00	–7.00	$He_3Li_3^+$	–10.82	–6.63	–6.68
NeH_3^+	–32.64	–2.01	–7.01	$NeLi_3^+$	–11.05	–6.73	–7.06
$Ne_2H_3^+$	–32.08	–1.92	–6.29	$Ne_2Li_3^+$	–11.07	–6.75	–6.86
$Ne_3H_3^+$	–31.74	–1.85	–5.67	$Ne_3Li_3^+$	–11.08	–6.77	–6.65
ArH_3^+	–26.16	–1.35	–4.26	$ArLi_3^+$	–11.01	–6.72	–6.80
$Ar_2H_3^+$	–25.95	–1.11	–2.66	$Ar_2Li_3^+$	–10.97	–6.72	–6.34
$Ar_3H_3^+$	–25.75	–0.98	–1.41	$Ar_3Li_3^+$	–10.93	–6.73	–5.84
KrH_3^+	–21.47	–1.01	–2.70	$KrLi_3^+$	–10.98	–6.71	–6.63
$Kr_2H_3^+$	–22.31	–0.60	–0.43	$Kr_2Li_3^+$	–10.92	–6.71	–6.01
$Kr_3H_3^+$	–22.37	–0.45	1.18	$Kr_3Li_3^+$	–10.87	–6.70	–5.34

Table 2. Total energy decomposition analysis for reactions as outlined below. Some plausible reactions that could occur due to the attack of noble gas atoms onto the equilateral triangle H_3^+/Li_3^+ moiety. Units are in kJ/mol.

	Reactions	ΔH	ΔE	ΔE_e	ΔE_s	ΔE_q	ΔE_{xc}	ΔT_s
				H_3^+				
1	$H_3^+ + He \rightarrow HeH_3^+$	–4.9	–7.5	–17.6	–193.8	203.9	–6.2	16.3
2	$HeH_3^+ + He \rightarrow He_2H_3^+$	–4.4	–6.6	–11.6	–169.5	174.6	–4.1	9.2
3	$He_2H_3^+ + He \rightarrow He_3H_3^+$	–3.9	–5.9	–10.8	–151.3	156.1	–3.8	8.7
4	$H_3^+ + Ne \rightarrow NeH_3^+$	–11.4	–13.9	–20.0	–238.3	244.4	–4.6	10.7
5	$NeH_3^+ + Ne \rightarrow Ne_2H_3^+$	–9.2	–11.4	–10.6	–208.0	207.2	–3.6	2.9
6	$Ne_2H_3^+ + Ne \rightarrow Ne_3H_3^+$	–7.9	–9.9	–7.4	–186.8	184.3	–3.7	1.2
7	$H_3^+ + Ar \rightarrow ArH_3^+$	–48.7	–48.2	–39.0	–349.4	340.3	–16.8	7.7
8	$ArH_3^+ + Ar \rightarrow Ar_2H_3^+$	–20.1	–23.4	–9.7	–243.4	229.8	–11.3	–2.3
9	$Ar_2H_3^+ + Ar \rightarrow Ar_3H_3^+$	–16.0	–18.3	–3.9	–199.4	185.0	–9.3	–5.1
10	$H_3^+ + Kr \rightarrow KrH_3^+$	–73.1	–68.6	155.3	–408.6	184.8	–25.1	–198.7
11	$KrH_3^+ + Kr \rightarrow Kr_2H_3^+$	–19.8	–24.7	132.7	–309.2	151.9	–10.7	–146.7
12	$Kr_2H_3^+ + Kr \rightarrow Kr_3H_3^+$	–17.2	–20.1	146.6	–239.3	72.6	–9.2	–157.5
				Li_3^+				
1	$Li_3^+ + He \rightarrow HeLi_3^+$	–1.4	–2.9	–12.6	–101.9	111.6	–4.7	14.4
2	$HeLi_3^+ + He \rightarrow He_2Li_3^+$	–1.2	–2.6	–11.9	–98.8	108.1	–4.8	14.1
3	$He_2Li_3^+ + He \rightarrow He_3Li_3^+$	–1.1	–2.5	–12.1	–93.2	102.8	–4.9	14.5
4	$Li_3^+ + Ne \rightarrow NeLi_3^+$	–5.1	–6.5	–9.8	–161.0	164.3	–4.8	8.1
5	$NeLi_3^+ + Ne \rightarrow Ne_2Li_3^+$	–4.7	–6.1	–4.2	–159.4	157.5	–4.7	2.8
6	$Ne_2Li_3^+ + Ne \rightarrow Ne_3Li_3^+$	–4.5	–5.9	–2.7	–159.0	155.8	–4.8	1.7
7	$Li_3^+ + Ar \rightarrow ArLi_3^+$	–12.1	–13.5	–3.1	–182.8	172.4	–7.7	–2.8
8	$ArLi_3^+ + Ar \rightarrow Ar_2Li_3^+$	–11.2	–12.6	0.0	–177.8	165.2	–7.9	–4.8
9	$Ar_2Li_3^+ + Ar \rightarrow Ar_3Li_3^+$	–10.2	–11.7	1.5	–173.2	160.0	–8.3	–4.9
10	$Li_3^+ + Kr \rightarrow KrLi_3^+$	–15.2	–16.6	153.5	–223.3	53.2	–6.9	–163.3
11	$KrLi_3^+ + Kr \rightarrow Kr_2Li_3^+$	–13.8	–15.2	177.6	–228.5	35.7	–6.9	–185.9
12	$Kr_2Li_3^+ + Kr \rightarrow Kr_3Li_3^+$	–12.4	–13.8	184.4	–224.6	26.4	–7.3	–191.0

Table 3. ITA quantities for chemical reactions in table 2. Atomic unit.

No.	ΔS_s	ΔI_F	ΔS_{GBP}	ΔI_G	No.	ΔS_s	ΔI_F	ΔS_{GBP}	ΔI_G
		H_3^+					Li_3^+		
1	–0.13	–0.59	0.90	–0.06	1	–0.10	–0.31	0.92	–0.06
2	–0.10	–0.52	0.90	–0.05	2	–0.10	–0.30	0.91	–0.06
3	–0.09	–0.46	0.91	–0.05	3	–0.10	–0.28	0.91	–0.05
4	–0.16	–0.73	3.76	–0.09	4	–0.11	–0.49	3.80	–0.09
5	–0.13	–0.63	3.75	–0.07	5	–0.11	–0.49	3.79	–0.09
6	–0.12	–0.57	3.76	–0.06	6	–0.12	–0.48	3.78	–0.08
7	–0.36	–1.06	5.49	–0.19	7	–0.17	–0.56	5.45	–0.13
8	–0.22	–0.74	5.37	–0.07	8	–0.18	–0.54	5.44	–0.12
9	–0.19	–0.61	5.40	–0.06	9	–0.19	–0.53	5.43	–0.11
10	–0.45	–1.24	9.99	–0.23	10	–0.19	–0.68	9.89	–0.15
11	–0.25	–0.94	9.77	–0.06	11	–0.20	–0.70	9.87	–0.13
12	–0.21	–0.73	9.82	–0.05	12	–0.21	–0.68	9.86	–0.11

Table 4. Correlation matrix (R) between the total energy, its components and the ITA quantities.

	ΔE	ΔT_s	ΔE_e	ΔE_{xc}	ΔE_s	ΔE_q	ΔS_s	ΔS_{GBP}	ΔI_F	ΔI_G	ΔH
ΔE	1.000										
ΔT_s	0.484	1.000									
ΔEe	–0.377	–0.993	1.000								
ΔExc	0.966	0.463	–0.363	1.000							
ΔE_s	0.925	0.575	–0.480	0.842	1.000						
ΔE_q	–0.359	0.571	–0.657	–0.292	–0.342	1.000					
ΔS_s	0.973	0.579	–0.482	0.960	0.926	–0.252	1.000				
ΔS_{GBP}	–0.577	–0.892	0.866	–0.546	–0.690	–0.331	–0.693	1.000			
ΔI_F	0.925	0.575	–0.480	0.842	1.000	–0.342	0.926	–0.690	1.000		
ΔI_G	0.759	0.438	–0.361	0.736	0.661	–0.147	0.783	–0.534	0.661	1.000	
ΔH	0.997	0.474	–0.366	0.966	0.902	–0.346	0.965	–0.553	0.902	0.790	1.000